scientific reports

Check for updates

OPEN

Identification of necroptosis-related gene signatures for predicting the prognosis of ovarian cancer

Yuling Qin[1,3], Yawen Sheng[2,3], Mengxue Ren[1], Zitong Hou[1], Lu Xiao[1] & Ruixue Chen[1✉]

Ovarian cancer (OC) is one of the most prevalent and fatal malignant tumors of the female reproductive system. Our research aimed to develop a prognostic model to assist inclinical treatment decision-making.Utilizing data from The Cancer Genome Atlas (TCGA) and copy number variation (CNV) data from the University of California Santa Cruz (UCSC) database, we conducted analyses of differentially expressed genes (DEGs), gene function, and tumor microenvironment (TME) scores in various clusters of OC samples.Next, we classified participants into low-risk and high-risk groups based on the median risk score, thereby dividing both the training group and the entire group accordingly. Overall survival (OS) was significantly reduced in the high-risk group, and two independent prognostic factors were identified: age and risk score. Additionally, three genes—C-X-C Motif Chemokine Ligand 10 (CXCL10), RELB, and Caspase-3 (CASP3)—emerged as potential candidates for an independent prognostic signature with acceptable prognostic value. In Gene Ontology (GO) and Kyoto Encyclopedia of Genes and Genomes (KEGG) enrichment analyses, pathways related to immune responses and inflammatory cell chemotaxis were identified. Cellular experiments further validated the reliability and precision of our findings. In conclusion, necroptosis-related genes play critical roles in tumor immunity, and our model introduces a novel strategy for predicting the prognosis of OC patients.

Keywords Ovarian cancer, Necroptosis, Signatures, Prognosis

Abbreviations

OC	Ovarian cancer
TCGA	The Cancer Genome Atlas
CNV	Copy number variation
UCSC	University of California Santa Cruz
DEGs	Differentially expressed genes
TME	Tumor microenvironment
OS	Overall survival
CXCL10	C-X-C Motif Chemokine Ligand 10
CASP3	Caspase-3
GO	Gene ontology
KEGG	Kyoto encyclopedia of genes and genomes
RIPK	Receptor-interacting protein kinase
MLKL	Mixed lineage kinase domain like pseudokinase
NR Genes	Necroptosis-related genes
GEO	Gene expression omnibus
CDF	Cumulative distribution function
GSEA	Gene set enrichment analysis

[1]Guang'anmen Hospital, China Academy of Chinese Medical Sciences, No. 5, Beixiange Road, Xicheng District, Beijing 100053, China. [2]Shandong University of Traditional Chinese Medicine, Jinan 250014, Shandong, China. [3]These authors contributed equally: Yuling Qin and Yawen Sheng. ✉email: crx1602@163.com

Ovarian cancer (OC) is frequently diagnosed at an advanced stage, which contributes to its high mortality rates. In 2020, there were approximately 314,000 new cases and over 207,000 deaths worldwide[1,2]. Currently, the most common treatments for OC are surgery and chemotherapy; however, the low survival and high recurrence rate continue to confound the medical community. Consequently, new treatment modalities, such as targeted therapy or immunotherapy, are imperative[3]. The purpose of this study was to develop a prognostic model for OC to facilitate more effective targeted therapies.

Necroptosis is a novel programmed cell death pathway characterized by significant inflammatory outcomes and immune responses. It differs from apoptosis, and its common symptoms include cellular swelling, organelle dysfunction, extensive mitochondrial damage, and plasma membrane rupture[4,5]. Necroptosis is dependent on receptor-interacting protein kinase 1 (RIPK1), RIPK3, and mixed lineage kinase domain like pseudokinase (MLKL) from a morphological standpoint[6,7]. According to studies, necroptosis may play crucial roles in tumorigenesis and also has tumor-suppressing effects[8,9]. However, the relationship between necroptosis and OC remains unclear. In order to predict the prognosis of OC, we performed a novel necroptosis-related gene signatures analysis. Using high-throughput sequencing technology and bioinformatics analysis, researchers can screen out a large number of Necroptosis-related Genes (NR Genes) from ovarian cancer tissues in recent research. These NR Genes are likely to be closely related to the occurrence and development of ovarian cancer. We can gain a deep understanding of their biological functions and prognosis in ovarian cancer through further functional annotation and enrichment analyses of these NR Genes. The advancement of interaction prediction research in various fields of computational biology would provide valuable insights into genetic markers related with OC in recent years[10,11].

Materials and methods
Data collection
We acquired gene expression and clinical information of 379 cancer samples from TCGA (https://tcga-data.nci.nih.gov/tcga/). Raw TCGA data is subjected to an ID transformation. Then, genes associated with necroptosis were retrieved from previous research and the published literature. In addition, TCGA provides mutation data as supplementary information. CNV data were downloaded from the UCSC database (http://genome.ucsc.edu/). In addition, GSE140082 was downloaded from the Gene Expression Omnibus (GEO) database as an external cohort for validation.

Visualization of necroptosis-related genes and CNVs
It's been demonstrated that CNVs can predict different tumor subtypes[12]. The collected CNVs genes exhibited copy loss and copy gain variants, and we then evaluated the CNVs at the level of the 23 chromosomes[13,14]. Mutation annotation format (MAF) data were processed and analyzed using the MutSigCV algorithm and the"mafools" software package. A waterfall plot was used to visualize the mutational information of NR Genes from OC patients in the TCGA database. The CNV frequency figures were visualized using the "barplot" command in the R language. The ordinate represented the frequency of the CNV that corresponded to NR Genes, and the abscissa represented the name of NR Genes. Circles of CNV frequencies were drawn using the "RCircos" package (Red: high frequency of increased NR Genes copy number; Blue: high frequency of deleted NR Genes copy number).

Consensus clustering analysis
Consensus clustering analysis of OC samples was performed using both "limma" and "consensusClusterPlus" packages based on euclidean distance and Wards linkage. Initially, 379 cancer samples were divided into k-clusters. The quantitative stability evidence was obtained based on cumulative distribution function (CDF) in order to further confirm the optimal number of clusters. Next, the identified k clusters and actual patient prognosis were evaluated using the Kaplan–Meier and progression-free survival curves. Based on the sample expression level of OC patients in the TCGA database, the matrix scores and immunity scores were calculated using the "ESTIMATE" package among genotypes. In order to quantify and analyze the immune cell infiltration levels of each genotyping sample, the "CIBERSORT" computational R package was used to plot heat maps and pairwise difference plots. Gene function and differentially expressed genes studies were performed for every cluster. The ClueGo plugin in Cytoscape (3.9.0) was used to do a functional analysis of DEGs, using a threshold of $p < 0.05$.

Establishment and validation of the risk signature
Half of the 379 cancer samples were chosen at random as the train group using Strawberry Perl and the caret R package. Initially, a Univariate Cox analysis was performed on the necroptosis-related gene signature in the train group to identify prognosis-related genes ($p < 0.05$)[15,16]. Then, the optimal Log(λ) value was determined using LASSO regression analysis with tenfold cross-validation[17–22], and a gene signature was constructed accordingly[23,24]. To validate our signature, the entire group was utilized in order to confirm the prognostic signature. Risk score $\sum_{i=1}^{n} expi \times ci = \sum_{i=1}^{n} expi \times ci$ (where n, expi, and ci represent the number of prognostic genes, the expression value, and the coefficient of gene I respectively. The patients were then split into high-risk and low-risk groups based on the median value of the risk score, the OS of the two risk subgroups was analyzed and compared using the "survival" package. In addition, Kaplan–Meier curves and multivariable analyses identified independent prognostic factors[25,26]. A risk heat map, a risk curve, ROC curve analysis[27,28], and survival analysis were performed for our signature[29,30]. For extra validation, we also used an independent external dataset (GSE140082). GO/KEGG enrichment analysis[31–33] of DEGs was performed using the clusterProfiler R package[34,35], and we used gene set enrichment analysis (GSEA) to investigate significantly enriched pathways in the high-risk and low-risk groups. Additionally, we contrasted m6A-related genes, immune activity, survival rates, and other factors.

Cell culture

Sk-ov-3 human ovarian cancer cell line, purchased from Shanghai Fu Heng Biological Co. The cells were cultured in DMEM + 10% FBS medium (both purchased from gibco) at 37℃, 5% CO2, pH 7.2–7.4, at a sterile constant temperature. The cells were passaged when the cell fusion reached 90%.

CCK8

Necrostatin-1 (Nec-1) is a potent inhibitor of necroptosis, purchased from MedChemExpress. The sk-ov-3 cells were inoculated 24 h in advance in 96-well plates at a density of 5000 cells/well, and after one day and night of complete cell wall attachment, the cells were replaced with serum-free medium with or without 100 nM Nec-1 and incubated for 24 h with the cck8 Cell Activity Kit (The absorbance at 450 nm was measured using the cck8 cell activity kit (purchased from Shanghai Toyobo Biotechnology Co., Ltd.).

Results

The research fow of this paper is shown in Fig. 1.

Necroptosis-related genes and CNVs in OC patients

Finally, 379 cancer samples from TCGA and UCSC were used to extract 76 necroptosis-related genes, including NLRP3, TLR4, and IRF6 (Fig. 2A). Then, we calculated the frequency of CNV status (gain/loss) and discovered that CNV loss was more prevalent overall (Fig. 2C) (red: gain; green: loss). CNV is a structural variation in chromosome that can lead to amplification or deletion of a section of chromosome; therefore, to pinpoint the location of variations on 23 chromosomes, a heatmap was created (Fig. 2B). In the graph, CNVs are displayed at a maximum of the region of human chromosomes 1 and 6.
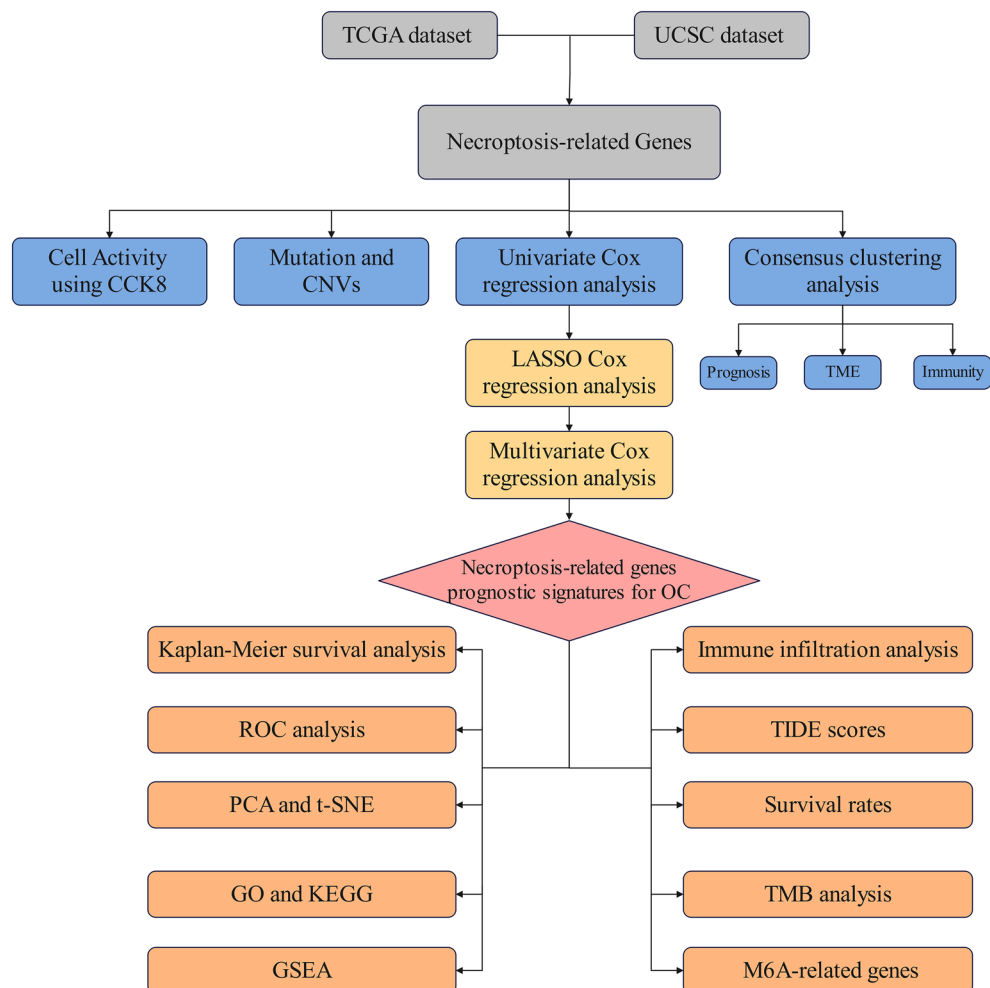

Figure 1. Flow diagram of full-text data.
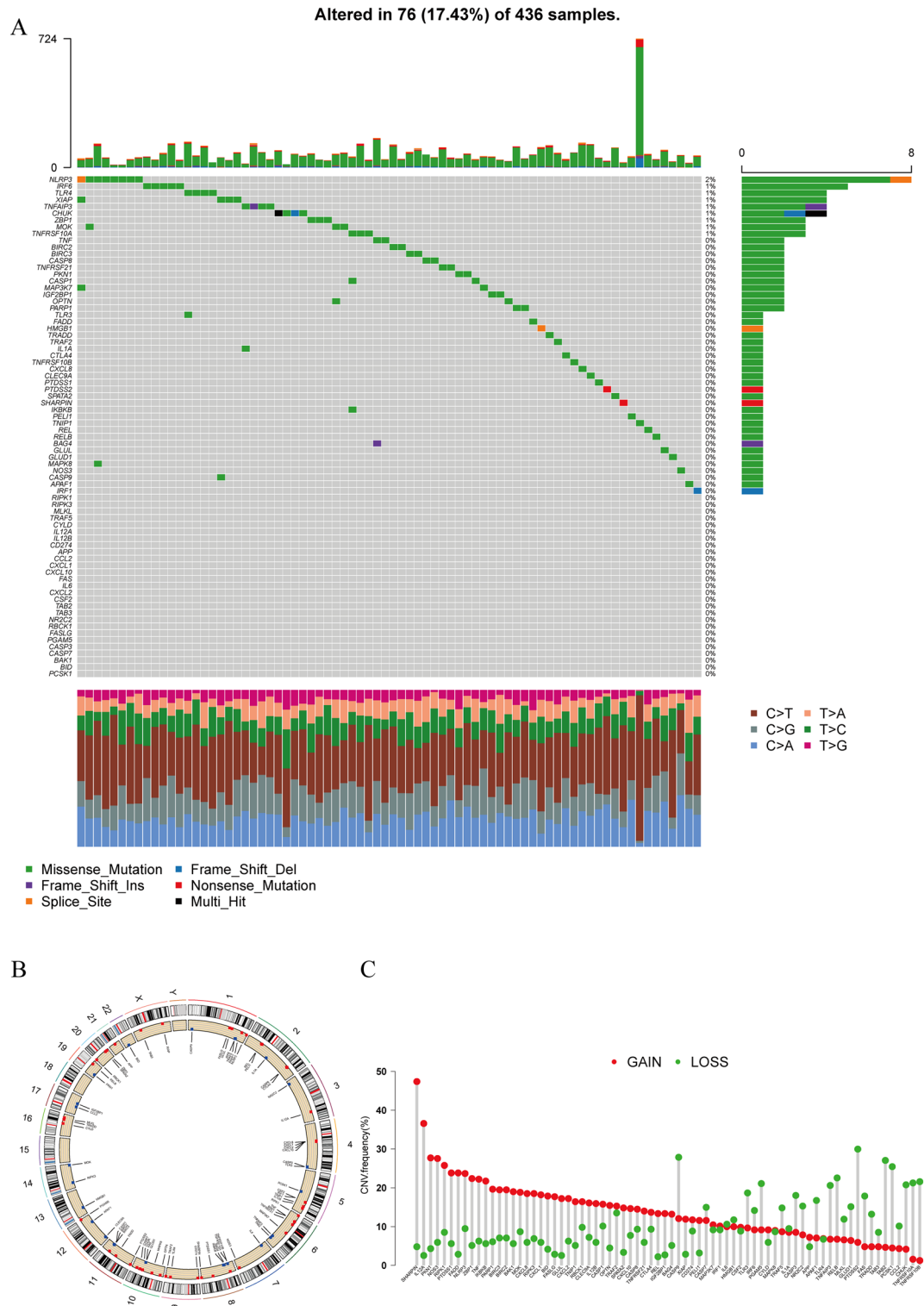
Figure 2. Genes and CNVs associated with necroptosis in OC. (**A**) Identified 76 genes related to necroptosis in OC samples. (**B**) The position of variations on 23 chromosomes. (**C**) The frequency of CNV (gain/loss) status.

Cancer classification

Using the CDF of the consensus index, we calculated the consensus matrix for each value of k by increasing the clustering variable (k) from 2 to 9. This allowed us to use all 379 OC patients from the TCGA to define the associations between the expression of 76 genes related to necroptosis and OC classifications. The greatest value, k = 3, showed that 379 OC patients could be grouped into three groups (Fig. 3A–C). Figure 3D illustrates the minimal variations in immune cell expression levels among the three clusters, while Fig. 3E displays the
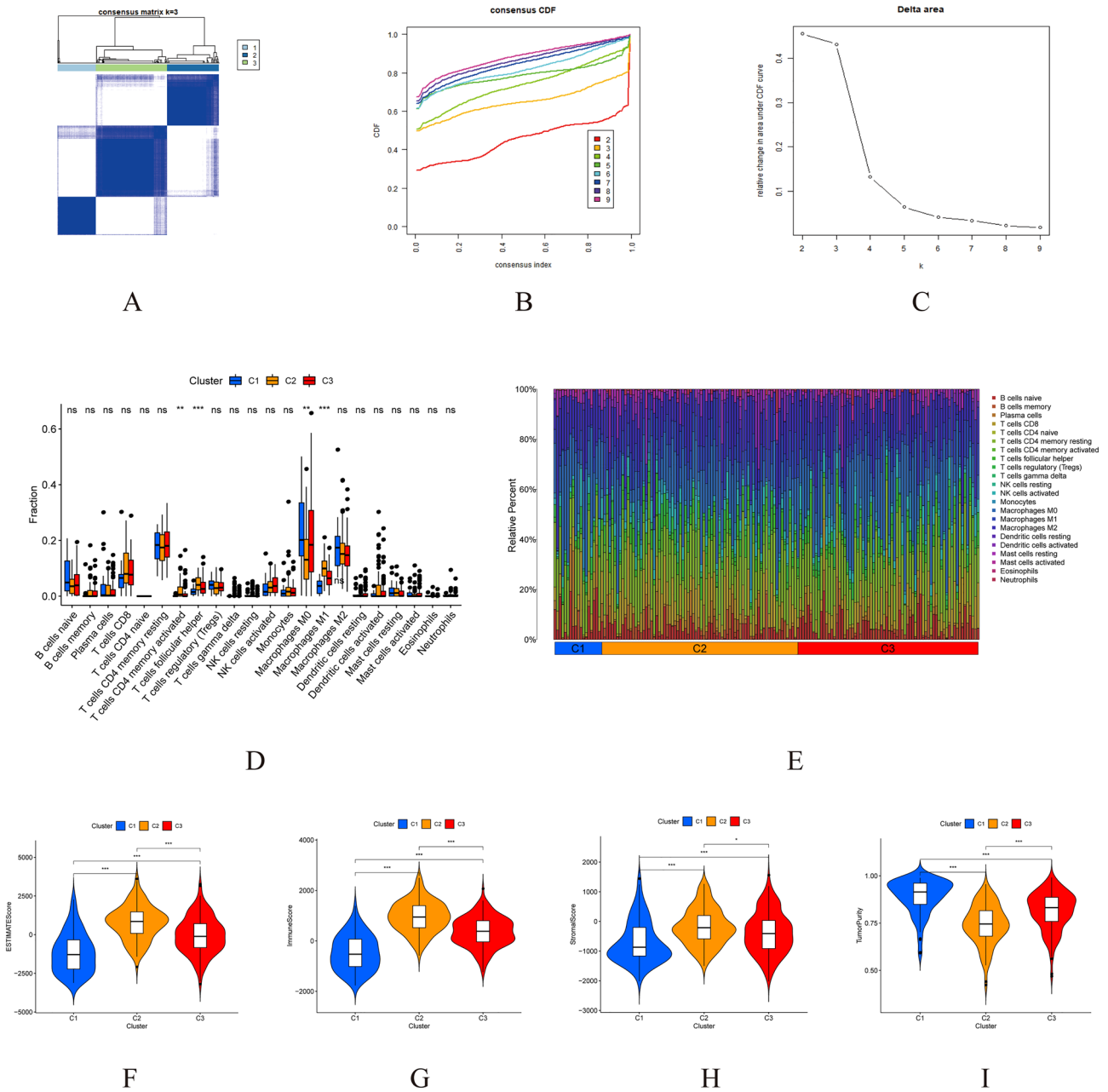
Figure 3. Comparisons of the 76 necroptosis-related genes into three clusters. (**A–C**) Using the CDF to determine K-cluster. (**D**) Immune cell expression in three clusters. (**E**) The proportion of various immune cells present in these clusters. (**F–I**) TME scores of three clusters.

percentage of unique immune cells inside each cluster. Tumor purity and TME scores (immune, stromal, and estimation scores) for three clusters are shown in Fig. 3F–I. Figure 4A displays the functional analysis results of a differentially expressed genes conducted to better understand the differences among three clusters. According to the Kaplan–Meier analysis (Fig. 4B, p < 0.001), cluster 3 had a significantly better survival probability than the other clusters. In cluster 3, CXCL10 expression was particularly high, while no other gene showed any specificity (Fig. 4C).

Construction and verification of the model

On the basis of clinical OC cases from the TCGA, prognosis-related genes were analyzed using univariate Cox proportional hazard regression analysis (p < 0.05). Due to the possibility of overfitting problems in the prognostic model, the Lasso regression with tenfold cross-validation was employed (Fig. 5A,B). The following formula was used to calculate the risk score for OC patients: risk score = CXCL10 × (− 0.186741112236078) + RELB × (0.669 433208748248) + CASP3 × (− 0.285126720445466).

A comparison of risk scores, principal component analysis (PCA), tSNE analysis, survival time, and Kaplan–Meier survival curves of OS (survival probability) of OC patients were made between high- and low-risk
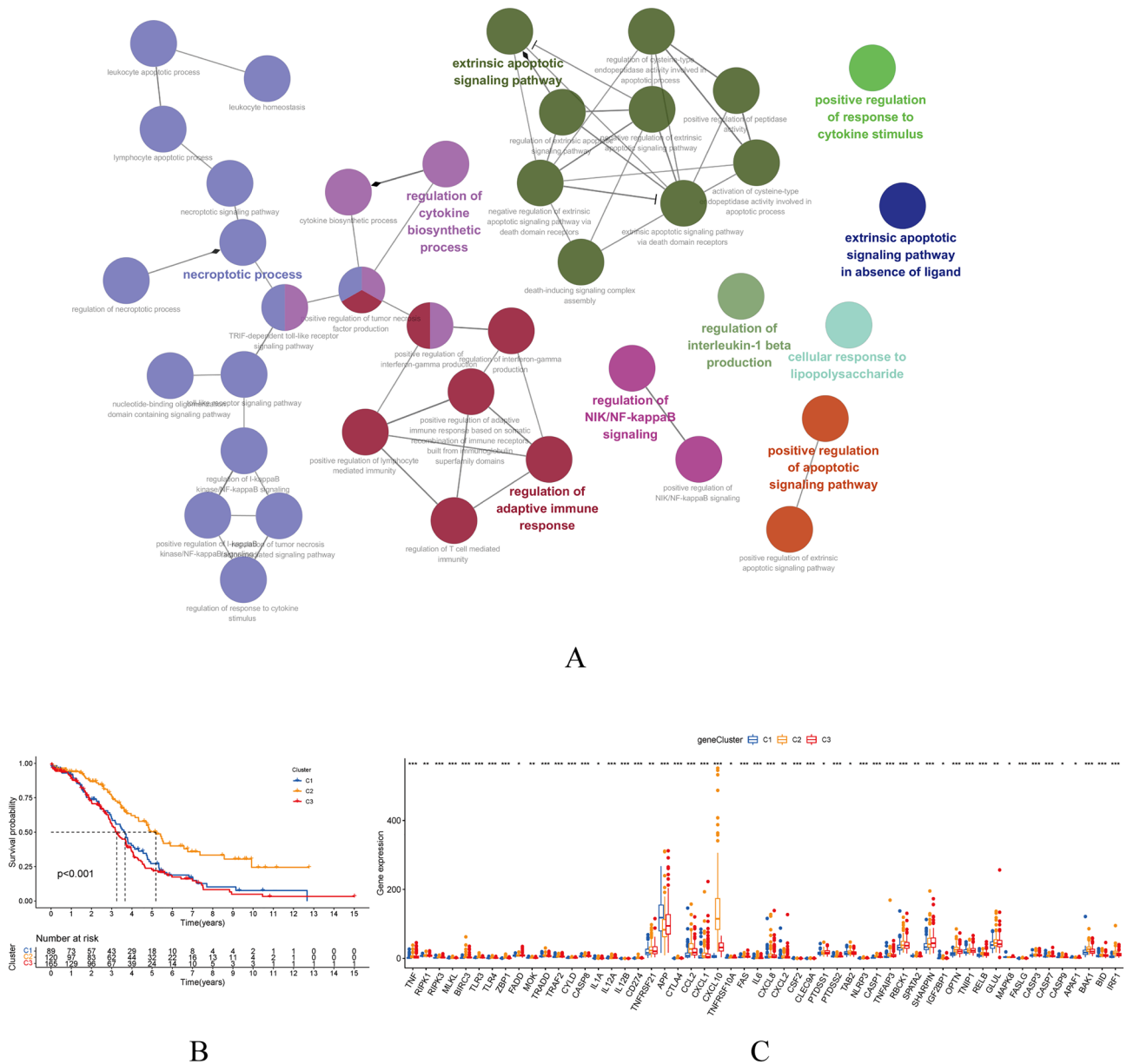
Figure 4. (**A**) Functional Analysis of the differentially expressed genes (DEGs) of three clusters. (**B**) Probability of survival in the three clusters. (**C**) The levels of gene expression in three clusters.

groups in the train and the entire group (Fig. 5C–L). The median risk score was utilized to create high- and low-risk subgroups. The group with the lowest risk had a better prognosis than the groups with the highest risk, according to these figures.. Relevant gene expression differences between the two groups were also observed (Fig. 5M,N). Furthermore, We added an additional validation set (GSE140082) with a survival curve illustrating that the high-risk group is detrimental to patient prognosis (Supplementary Fig. 1) and a ROC curve illustrating its good predictive value (Supplementary Fig. 2).

Construction of nomogram

It was discovered that age and risk score were independent prognostic factors. The hazard ratio (HR) and 95 percent confidence interval (CI) for age and risk score are as follows:: risk score 1.460 (1.227–1.738) (p < 0.001) in univariate Cox (uniCox) regression and 1.419 (1.192–1.691) (*p* < 0.001) in multivariate Cox (multi-Cox) regression, respectively; age in uniCox regression (1.022 and 1.010–1.035; *p* < 0.001) and age in multivariate Cox regression (1.020 and 1.008–1.033; *p* = 0.002) (Fig. 6A,B). Tumor grade was excluded as a prognostic factor since its p value was not less than 0.05.

Two independent factors (risk score and age) were used to develop a nomogram for predicting the 1-, 3-, and 5-year OS incidences of OC patients (Fig. 6C). We also constructed 1-, 3-, and 5-year calibration plots to confirm that the nomogram accurately predicted 1-, 3-, and 5-year OS (Fig. 6D).
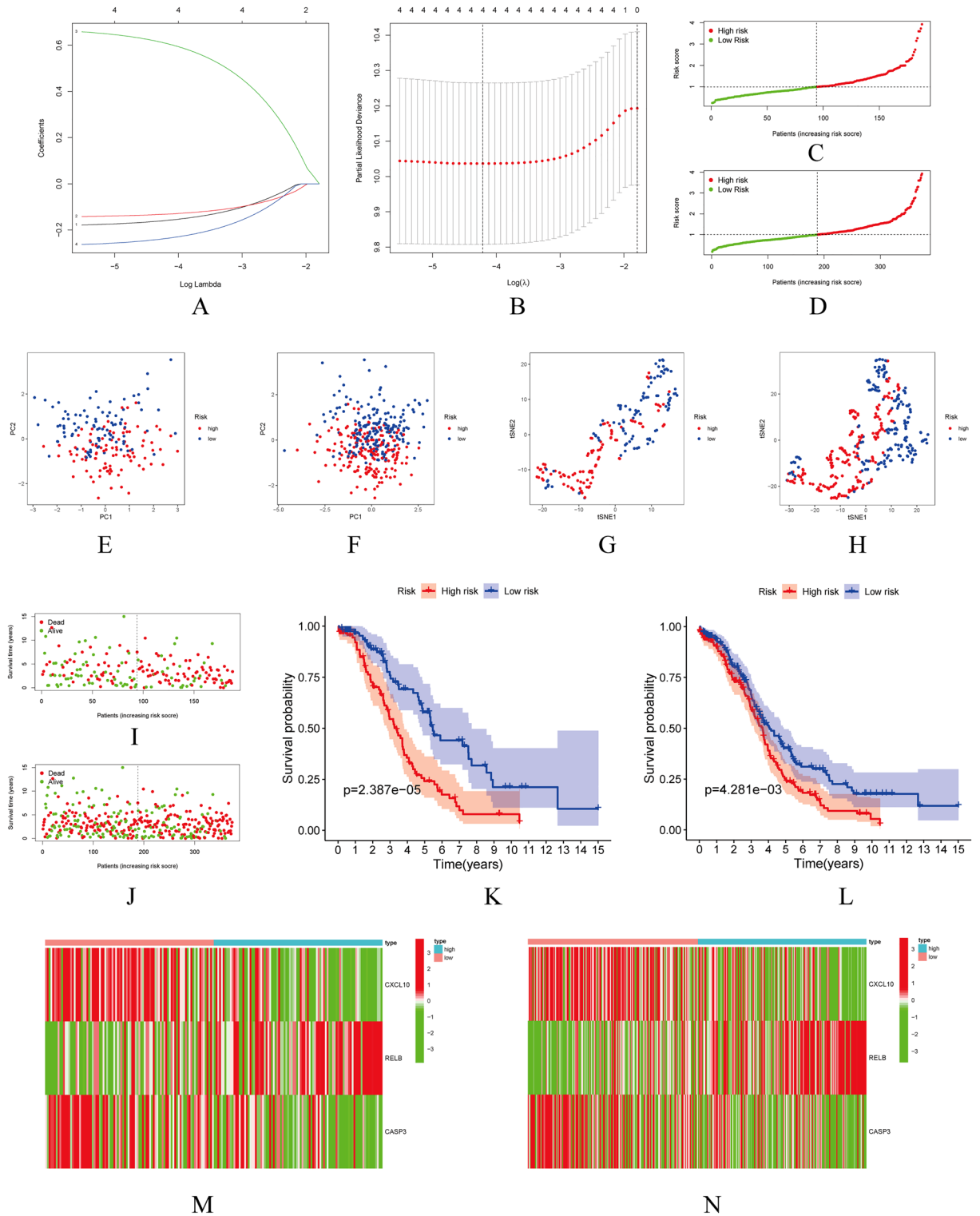
Figure 5. Demonstrates the construction and prognostic value of the three necroptosis-related gene models in the train and entire groups. (**A**) Cross-validation performed 10 times for variable selection in the LASSO model. (**B**) LASSO coefficient profile of three genes associated with necroptosis. (**C,D**) Risk scores for the train and the entire group. (**E,F**) The train and entire groups' principal component analysis (PCA). (**G,H**) The tSNE analysis, between the train's high- and low-risk groups and the entire group. (**I,J**) Survival rate of OC patients in the train and the entire group. (**K,L**) OS (survival probability) Kaplan–Meier survival curves between high- and low-risk groups in the train and the entire group. (**M,N**) Expression of three relevant genes in the train and the entire group.
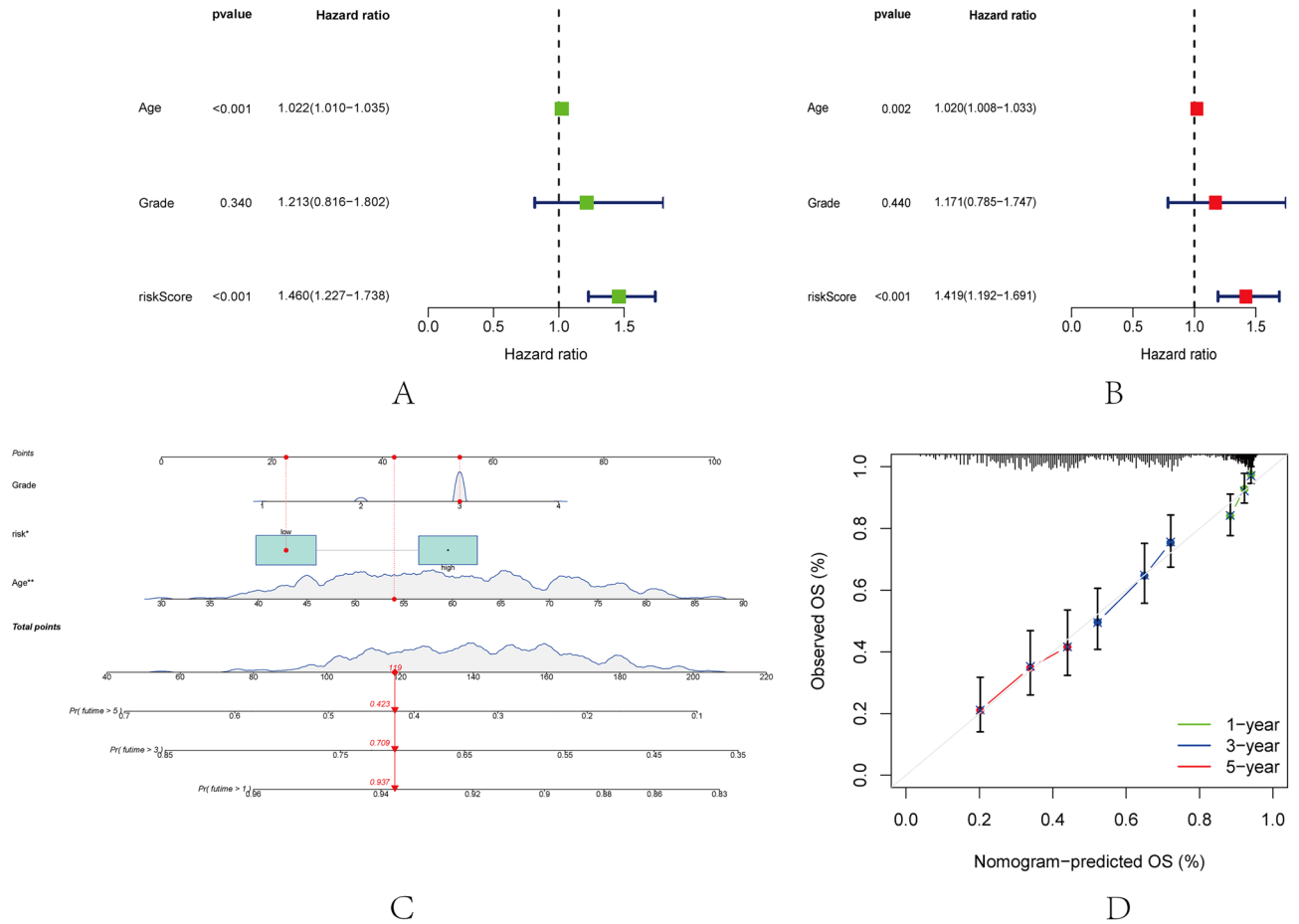
Figure 6. The risk model nomogram. (**A,B**) Univariate and multivariate Cox regression analyses of clinical factors (age, grade) and risk score. (**C**) Nomogram incorporating independent variables (risk score and age) for predicting the 1-, 3-, and 5-year incidences of OS in OC patients. (**D**) 1-year, 3-year, and 5-year OS calibration plots.

Independent prognostic value of the risk model

The univariate Cox regression analysis and multivariate Cox regression analysis were performed to evaluate whether the prognostic risk score model could be used as an independent prognostic predictor. Both univariate Cox regression analysis and multivariate Cox regression analysis showed that the age, grades, and risk scores can be used as independent prognostic factors when assessing patients with OC. ROC curves were generated to validate the accuracy of the prognostic model, and the area under the ROC curve (AUC) could be used to illustrate the results of ROC curves[36]. The 1-, 2-, and 5-year AUC for the train group were 0.707, 0.720, and 0.709, respectively, while those for the entire group were 0.598, 0.596, and 0.628, respectively (Fig. 7A,B). Clinical ROC curve analysis proved that the clinical factor: age (0.711) has greater predictive ability than other clinical factors (Fig. 7C).

Functional analyses of DEGs and gene set enrichment analysis (GSEA)

A differential gene KEGG and GO pathway enrichment analysis was conducted to gain a more comprehensive comprehension of the differences in gene functions and pathways between the high-risk and low-risk groups of the entire group. The DEGs were primarily associated with "immunoglobulin complex," "antigen binding," "immune response," "viral protein interaction with cytokine and cytokine receptor," "chemokine signaling pathways," and "cytokine-cytokine receptor interaction," according to our findings (Fig. 8A,B).

Additionally, we used GSEA to compare the two groups within the KEGG pathway for the entire group. In consequence, "adherensjunction", "adipocytokine", "ecm receptor interaction" "hedgehog signaling pathway", "inositol phosphate metabolism", and "tight junction" were significantly activated in high-risk patients (Fig. 8C–H).

Immune activity in risk groups and m6a-related genes

In the high-risk and low-risk groups, respectively, the two genes with the highest number of mutations were TP53 and TTN (Fig. 9A,B).

Immune cell infiltration plays a crucial role in tumor progression[37–39]. Using the single-sample gene set enrichment analysis(ssGSEA), we compared the level of immune-related pathways and functions between the
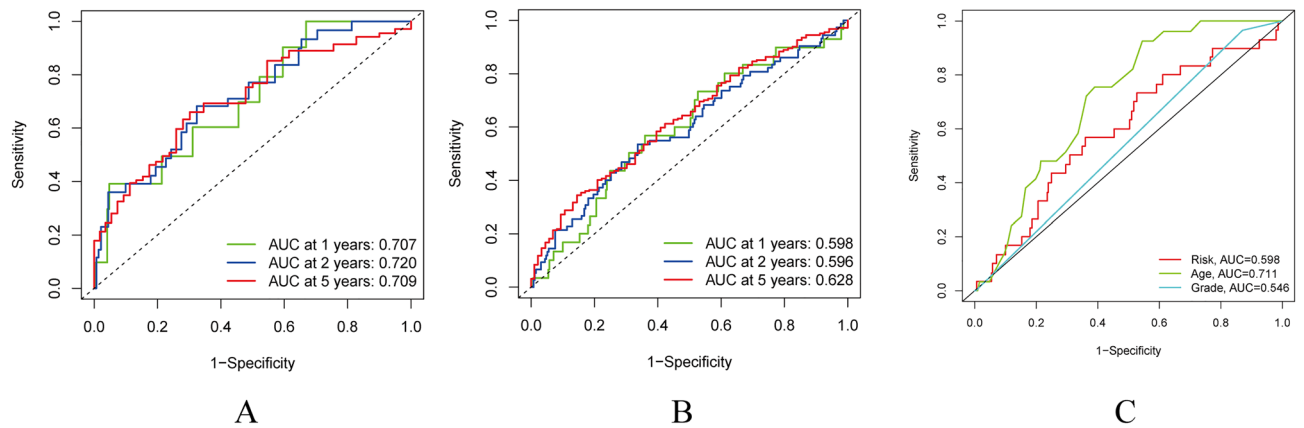
Figure 7. Evaluation of the risk model. (**A,B**) The area under the ROC curve (AUC) at 1 year, 2 years, and 5 years of the train and entire groups. (**C**) The risk score, age, and grade ROC curves.

high- and low-risk TCGA groups. Except for the induced dendritic cells (iDCs), the results showed that the high-risk group had nearly lower levels of immune cell infiltration than the low-risk group (Fig. 9C). In addition, there were notable differences between the two groups in terms of APC coinhibition, APC costimulation, cytokine-cytokine receptor (CCR), checkpoint, cytolytic activity, human leukocyte antigen (HLA), inflammation-promoting, MHC class I, parainflammation, T-cell coinhibition, T-cell costimulation, typeIFN response and typeIIFN response (Fig. 9D).

In addition, TME (including immune, stromal, and estimate scores) and m6A-related genes play a crucial role in the progression of tumors[40,41]. The TME scores in the high-risk group were lower, as shown in Fig. 8E. And we found that expression levels of immune scores had a negative correlation with risk score (p < 0.05), whereas stromal scores had little bearing on risk score according to our risk model (Fig. 9F,G).

Regarding m6A-related genes, the high-risk group had higher levels of METTL3, YTHDF1, RBM15, and ZC3H13 than the low-risk group (Fig. 9H).

Except for CD200, the expression of all immune checkpoints was nearly greater in the high-risk group than in the low-risk group (Fig. 9I). In addition, the TIDE score could simulate tumor immune evasion, which was more prevalent in the high-risk group compared to the low-risk group (Fig. 9J).

CCk-8 results

In addition, we used cck8 Cell Activity Kit to evaluate the activity of ovarian cancer cells by the appended Nec-1. CCk-8 results showed an increase in absorbance at 450 nm and enhanced activity of ovarian cancer cells after the addition of Nec-1, an inhibitor of necrotic apoptosis (Fig. 10).It seems reasonable to speculate that necroptosis may play crucial roles in the progress of OC.

Discussion

OC is a malignant gynecologic tumor with a poor prognosis and a high mortality rate, and surgery is generally the first-line treatment[42]. Patients with extensive metastatic deposits and malignant ascites in the enterocoelia, which cannot be treated surgically, are frequently not diagnosed until the disease has progressed to an advanced stage[43,44]. The 5-year survival rate for patients with advanced-stage ovarian cancer is less than 50%[45].

Necroptosis is a type of programmed cell death that is caspase-independent and distinct from apoptosis. It is mediated by death receptors such as receptor-interacting protein kinase (RIP) 1, TNF receptor 1, and RIP3, which cause necroptosis by activating the kinase domain-like protein (MLKL) to form necrosomes[46–48].

Bioinformatics technology has been steadily advancing and developing over the past few years. Prognostic prediction of cancer by building the prognostic model contributes to the clinical treatment of patients. Studies have demonstrated that necroptosis can inhibit the development and occurrence of tumors, particularly colorectal cancer and breast cancer[49]. Additionally, it can promote inflammatory death and create a microenvironment conducive to the growth of tumor cells, thereby promoting tumor growth. According to research, RIPK1 inhibitors can inhibit tumor growth and limit metastasis[50,51]. Overall, necroptosis has been shown to be a double-edged sword for tumor progression and a potential tumor therapy, specifically for drug-resistant tumors[52]. Our goal is to create a new prognostic model to evaluate the prognostic significance of genes related to necroptosis in OC.

Before their differences were identified by Kaplan–Meier analysis and differential gene expression analysis, 379 cancer samples in this study were divided into three clusters. Afterward, we constructed a prognostic model based on 76 necroptosis-related genes isolated from OC patients. Half of the patients were randomly assigned to the train group, and the entire group was used to validate. The comparisons revealed that the low-risk group had a more favorable prognosis than the high-risk group. After calculating each patient's risk score, two independent prognostic factors (risk score and age) were identified, and univariate Cox (uni-Cox), multivariate Cox (multi-Cox), nomogram, and calibration curves were used to validate and evaluate the model.

Three necroptosis-related genes, CXCL10, RELB, and CASP3, were identified in the prognostic model through multiple regression analyses. CXCL10 is one of the inflammatory chemokines, and the research has shown that
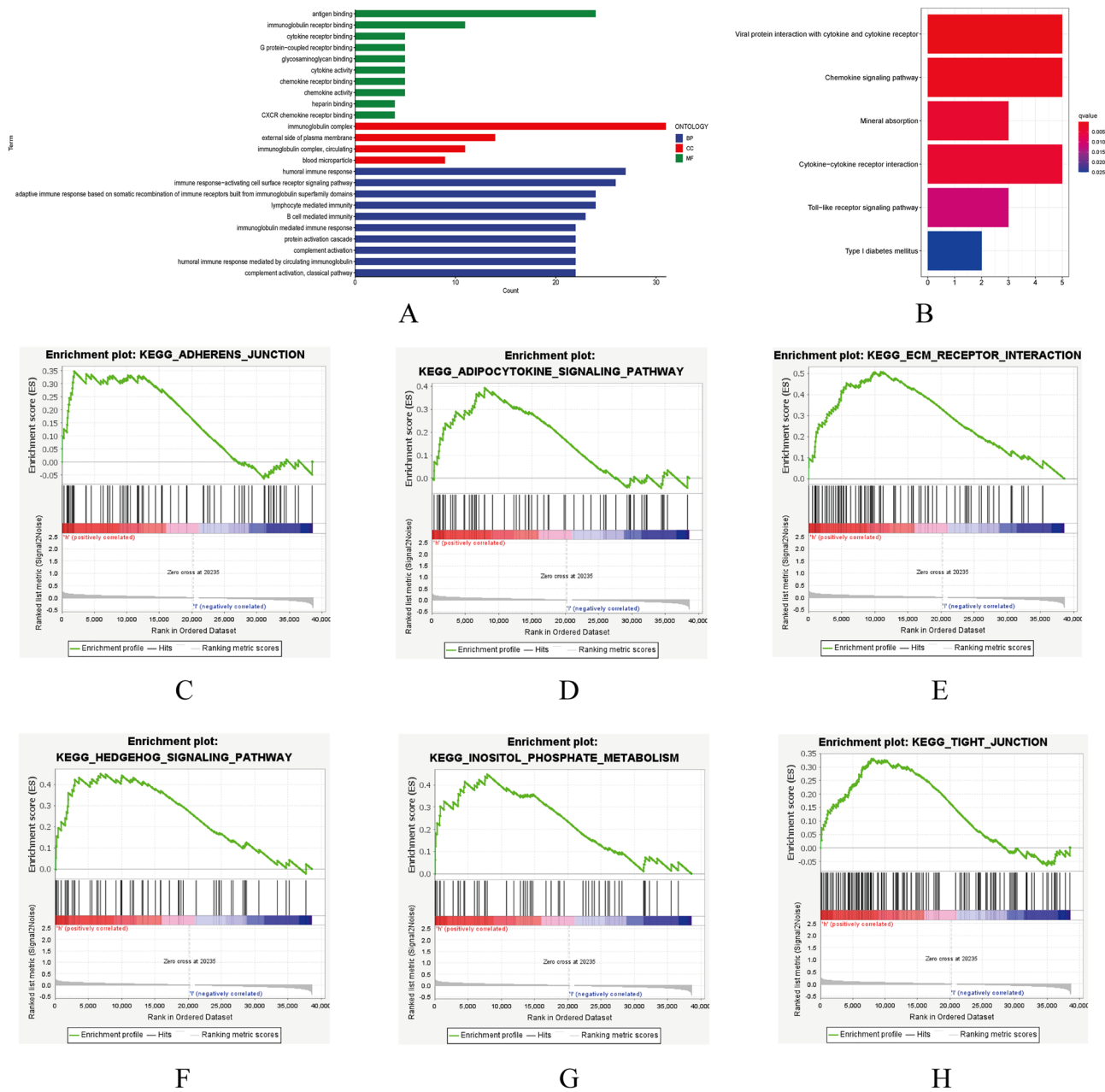
Figure 8. Functional analyses of DEGs and enrichment analysis of gene sets (GSEA). (**A,B**) Analysis of KEGG and GO enrichment pathways for DEGs in high- and low-risk groups. (**C–H**) The GSEA comparisons between high-risk and low-risk groups in the KEGG pathway for the entire group.

CXCL10 expression is crucial for ovarian cancer prognosis and TME immune characteristics[53]. Furthermore, CXCL10 was found to have an impact on angiogenesis in addition to stimulating T lymphocytes' ability to fight malignancies in the body[54]. According to some studies, CXCL10 regulates immunotherapy-sensitive tumors and is regarded as a biomarker of favorable prognosis[55]. In some studies, the level of RElB expression was associated with glioma, non-small cell lung cancer (NSCLC), and prostate cancer[56–58]. It has been demonstrated that CASPs, a group of proteases with similar structures, are involved in cell growth, cell differentiation, and apoptosis. Results indicated that CASP3 expression may improve the OS of patients with gastric cancer (GC)[59]. CASP3 is rarely expressed in various types of cancer, and CASP3 deficiency can cause cells to become resistant to microenvironmental stress and therapy[60]. However, additional research is necessary to determine how these genes interact during necroptosis.

The three necroptosis-related genes were used to construct a prognostic model with a decent prognostic value (0.707%, 0.720%, and 0.709% at 1, 2, and 5 years, respectively), and they can be considered prognostic biomarkers for OC. The GO and KEGG enrichment analyses revealed that the pathways were primarily associated with immune responses and inflammatory cell chemotaxis; therefore, it is reasonable to assume that necroptosis can regulate the infiltration of immune cells and the composition of the tumor immune microenvironment[61].
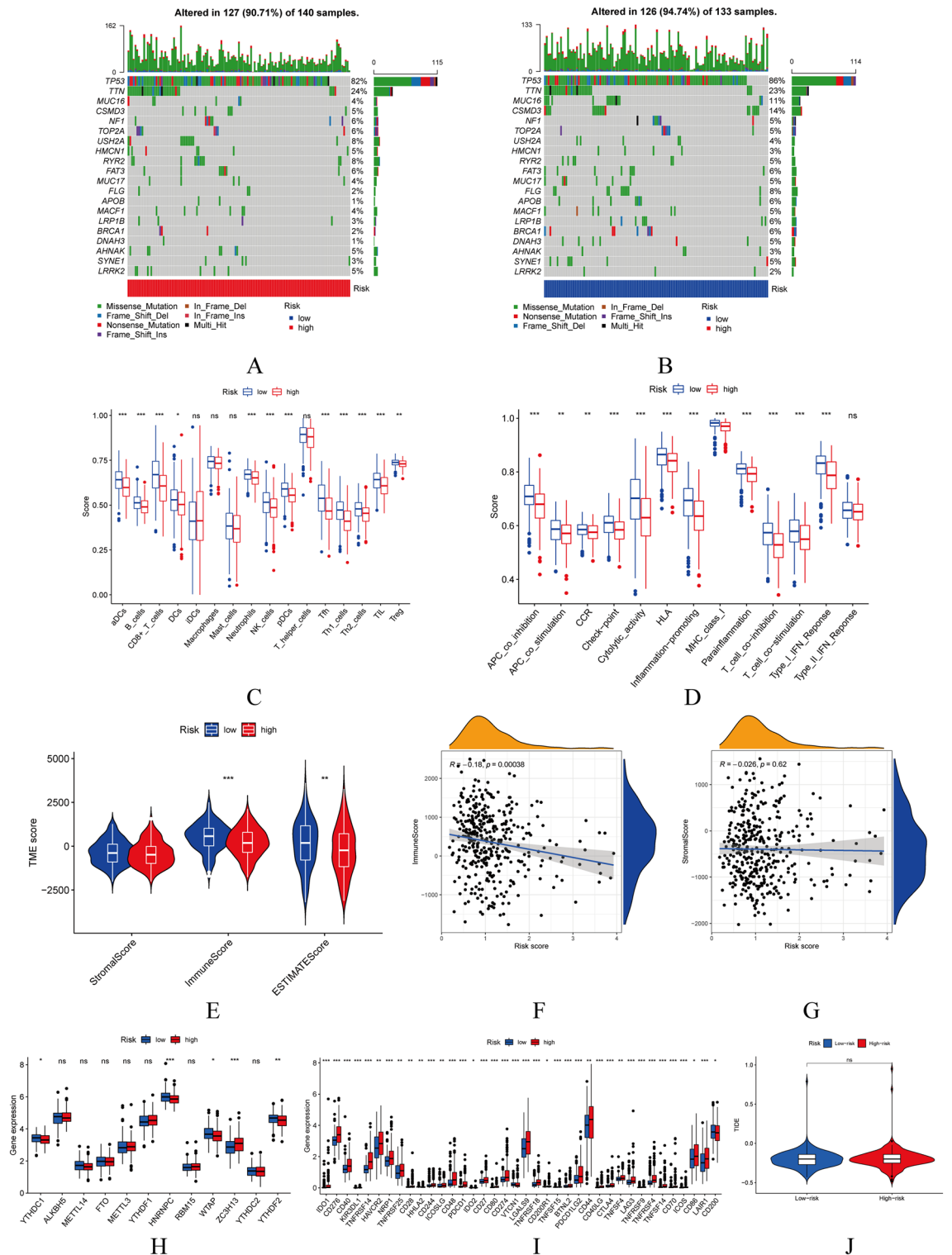
Figure 9. Immune activity in risk groups. (**A**,**B**) Variations in mutations between high- and low-risk groups. (**C**,**D**) Immune cell infiltration varies between high- and low-risk groups. (**E**) TME scores in the high- and low-risk groups. (**F**,**G**) Immune score and stromal score expression levels in high- and low-risk groups. (**H**–**J**) M6A-related genes, immune checkpoint expression, and TIDE scores in the high- and low-risk groups.

Limitations and future directions

Our study had limitations that must be taken into account. Firstly, the number of patients used in the study is small and there is a lack of health samples. The accuracy of our model needs to be validated in other external

Cell activity assay of SKOV-3
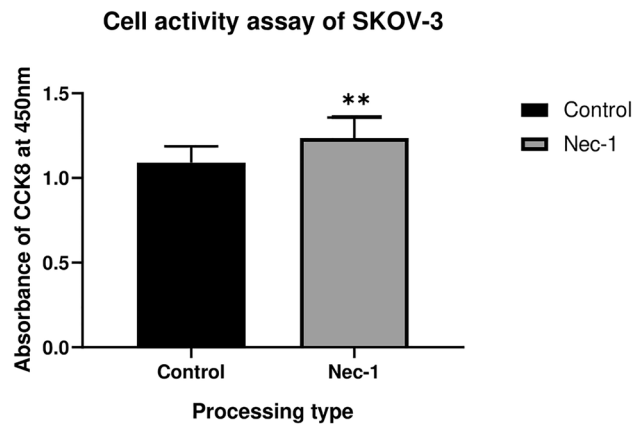
Figure 10. The Cell activity of SKOV-3 cells using the absorbance of CCK8 at 450 nm after the addition of Nec-1.

datasets and large clinical cohorts.

Computational biology has been evolving rapidly in recent years[62,63], the advancement of interaction prediction research in various fields of computational biology would provide valuable insights into genetic markers and related diseases[64,65], such as miRNA-lncRNA interaction prediction[66,67]. MicroRNAs (miRNAs) or long noncoding RNAs (lncRNAs) play important roles in biological activities, recent research has found that predicting the interaction between miRNA and lncRNA is the primary task for elucidating functional mechanisms[68,69]. In addition, ODE-based theoretical modeling studies on gene/protein signaling networks have been equally important for the study of understanding regulatory mechanisms and finding potential therapeutic targets in diseases[70–72].

Conclusion

In conclusion, the purpose of our study was to develop a prognostic model that would facilitate the formulation of clinical treatment decisions. We constructed a novel prognostic signature using three genes related to necroptosis in order to predict the prognosis of OC patients using multi-angle verifications, but the model did not have a very good predictive value. In the future, there is much work and further studies to be done in order to predict the prognosis and develop an accurate therapeutic strategy for the disease.

Data availability

Our data comes from public databases The Cancer Genome Atlas(TCGA) (https://portal.gdc.cancer.gov/). All the data in this paper support the results of this study.

Code availability

Supplementary Material.

References

1. Sung, H. *et al.* Global cancer statistics 2020: GLOBOCAN estimates of incidence and mortality worldwide for 36 cancers in 185 countries. *CA Cancer J. Clin.* **71**(3), 209–249 (2021).
2. Li, Y., Gong, X., Hu, T. & Chen, Y. Two novel prognostic models for ovarian cancer respectively based on ferroptosis and necroptosis. *BMC Cancer.* **22**(1), 74 (2022).
3. Zhao, Z. *et al.* Necroptosis-related lncRNAs: Predicting prognosis and the distinction between the cold and hot tumors in gastric cancer. *J. Oncol.* **2021**, 6718443 (2021).
4. Chen, D., Yu, J. & Zhang, L. Necroptosis: An alternative cell death program defending against cancer. *Biochim. Biophys. Acta.* **1865**(2), 228–236 (2016).
5. Liu, Z. G. & Jiao, D. Necroptosis, tumor necrosis and tumorigenesis. *Cell Stress.* **4**(1), 1–8 (2019).
6. Grootjans, S., Vanden Berghe, T. & Vandenabeele, P. Initiation and execution mechanisms of necroptosis: An overview. *Cell Death Differ.* **24**(7), 1184–1195 (2017).
7. Moujalled, D. M., Cook, W. D., Murphy, J. M. & Vaux, D. L. Necroptosis induced by RIPK3 requires MLKL but not Drp1. *Cell Death Dis.* **5**(2), e1086 (2014).
8. Rodriguez, D. A. *et al.* Characterization of RIPK3-mediated phosphorylation of the activation loop of MLKL during necroptosis. *Cell Death Differ.* **23**(1), 76–88 (2016).
9. Seifert, L. *et al.* The necrosome promotes pancreatic oncogenesis via CXCL1 and Mincle-induced immune suppression. *Nature.* **532**(7598), 245–249 (2016).
10. Hu, H. *et al.* Gene function and cell surface protein association analysis based on single-cell multiomics data. *Comput. Biol. Med.* **157**, 106733 (2023).
11. Wang, W., Zhang, L., Sun, J., Zhao, Q. & Shuai, J. Predicting the potential human lncRNA–miRNA interactions based on graph convolution network with conditional random field. *Br. Bioinform.* **23**(6), 463 (2022).
12. Zack, T. I. *et al.* Pan-cancer patterns of somatic copy number alteration. *Nat. Genet.* **45**(10), 1134–1140 (2013).

13. Zou, J. *et al*. A multi-omics-based investigation of the prognostic and immunological impact of necroptosis-related mRNA in patients with cervical squamous carcinoma and adenocarcinoma. *Sci. Rep.* **12**(1), 16773 (2022).
14. Zhao, J. *et al*. Construction of N-7 methylguanine-related mRNA prognostic model in uterine corpus endometrial carcinoma based on multi-omics data and immune-related analysis. *Sci. Rep.* **12**(1), 18813 (2022).
15. Lin, Z., Fan, W., Sui, X., Wang, J. & Zhao, J. Necroptosis-related LncRNA signatures for prognostic prediction in uterine corpora endometrial cancer. *Reprod. Sci.* **30**(2), 576–589 (2023).
16. Lin, Z., Sui, X., Jiao, W., Wang, Y. & Zhao, J. Exploring the mechanism and experimental verification of puerarin in the treatment of endometrial carcinoma based on network pharmacology and bioinformatics analysis. *BMC Complement. Med. Ther.* **22**(1), 150 (2022).
17. Wang, Y. *et al*. lncRNA DLEU2 acts as a miR-181a sponge to regulate SEPP1 and inhibit skeletal muscle differentiation and regeneration. *Aging (Albany NY).* **12**(23), 24033–24056 (2020).
18. Zheng, R. Z. *et al*. Initial CT-based radiomics nomogram for predicting in-hospital mortality in patients with traumatic brain injury: A multicenter development and validation study. *Neurol. Sci.* **43**(7), 4363–4372 (2022).
19. Li, X. Y. *et al*. m7G methylation-related genes as biomarkers for predicting overall survival outcomes for hepatocellular carcinoma. *Front. Bioeng. Biotechnol.* **10**, 849756 (2022).
20. Zhao, Z., Ding, Y., Tran, L. J., Chai, G. & Lin, L. Innovative breakthroughs facilitated by single-cell multi-omics: Manipulating natural killer cell functionality correlates with a novel subcategory of melanoma cells. *Front. Immunol.* **14**, 1196892 (2023).
21. Zheng, R. *et al*. Chinese admission warning strategy for predicting the hospital discharge outcome in patients with traumatic brain injury. *J. Clin. Med.* **11**(4), 974 (2022).
22. Ding, Y. *et al*. Single-cell sequencing analysis related to sphingolipid metabolism guides immunotherapy and prognosis of skin cutaneous melanoma. *Front. Immunol.* **14**, 1304466 (2023).
23. Lin, Z. *et al*. Necroptosis-related lncRNA signature predicts prognosis and immune response for cervical squamous cell carcinoma and endocervical adenocarcinomas. *Sci. Rep.* **12**(1), 16285 (2022).
24. Zhao, J. *et al*. Construction of a prognostic model of luteolin for endometrial carcinoma. *Am. J. Transl. Res.* **15**(3), 2122–2139 (2023).
25. Xing, J. *et al*. Examining the function of macrophage oxidative stress response and immune system in glioblastoma multiforme through analysis of single-cell transcriptomics. *Front. Immunol.* **14**, 1288137 (2024).
26. Liu, P. *et al*. Unraveling the intricacies of glioblastoma progression and recurrence: Insights into the role of NFYB and oxidative phosphorylation at the single-cell level. *Front. Immunol.* **15**, 1368685 (2024).
27. Zhao, Z. J. *et al*. Prognostic value of different computed tomography scoring systems in patients with severe traumatic brain injury undergoing decompressive craniectomy. *J. Comput. Assist. Tomogr.* **46**(5), 800–807 (2022).
28. Ge, Q. *et al*. Deciphering the suppressive immune microenvironment of prostate cancer based on CD4+ regulatory T cells: Implications for prognosis and therapy prediction. *Clin. Transl. Med.* **14**(1), e1552 (2024).
29. Lin, Z. *et al*. Decoding the tumor microenvironment and molecular mechanism: Unraveling cervical cancer subpopulations and prognostic signatures through scRNA-Seq and bulk RNA-seq analyses. *Front. Immunol.* **15**, 1351287 (2024).
30. Zhou, W., Lin, Z. & Tan, W. Deciphering the molecular landscape: Integrating single-cell transcriptomics to unravel myofibroblast dynamics and therapeutic targets in clear cell renal cell carcinoma. *Front. Immunol.* **15**, 1374931 (2024).
31. Zhao, Z. *et al*. Untargeted metabolomic profiling of cuprizone-induced demyelination in mouse corpus callosum by UPLC-Orbitrap/MS reveals potential metabolic biomarkers of CNS demyelination disorders. *Oxid. Med. Cell Longev.* **2021**, 7093844 (2021).
32. Zhao, Z. J. *et al*. Integrating lipidomics and transcriptomics reveals the crosstalk between oxidative stress and neuroinflammation in central nervous system demyelination. *Front. Aging Neurosci.* **14**, 870957 (2022).
33. Zhao, Z. J. *et al*. The gene coexpression analysis identifies functional modules dynamically changed after traumatic brain injury. *Comput. Math. Methods Med.* **2021**, 5511598 (2021).
34. Lin, Z. *et al*. Mechanism investigation and experiment validation of capsaicin on uterine corpus endometrial carcinoma. *Front. Pharmacol.* **13**, 953874 (2022).
35. Lin, Z., Fan, W., Yu, X., Liu, J. & Liu, P. Research into the mechanism of intervention of SanQi in endometriosis based on network pharmacology and molecular docking technology. *Medicine (Baltimore).* **101**(37), e30021 (2022).
36. Chen, F. *et al*. Necroptosis-related lncRNA to establish novel prognostic signature and predict the immunotherapy response in breast cancer. *J. Clin. Lab. Anal.* **36**(4), e24302 (2022).
37. Stockis, J., Roychoudhuri, R. & Halim, T. Y. F. Regulation of regulatory T cells in cancer. *Immunology.* **157**(3), 219–231 (2019).
38. Wu, Y. *et al*. Development of an individualized ubiquitin prognostic signature for clear cell renal cell carcinoma. *Front. Cell Dev. Biol.* **9**, 684643 (2021).
39. Zhou, X., Liu, C., Zeng, H., Wu, D. & Liu, L. Identification of a thirteen-gene signature predicting overall survival for hepatocellular carcinoma. *Biosci. Rep.* **41**(4), BSR20202870 (2021).
40. Duan, J., Zhang, J. G., Deng, H. W. & Wang, Y. P. Comparative studies of copy number variation detection methods for next-generation sequencing technologies. *PLoS One.* **8**(3), e59128 (2013).
41. Lee, H., Na, K. J. & Choi, H. Differences in tumor immune microenvironment in metastatic sites of breast cancer. *Front. Oncol.* **11**, 649004 (2021).
42. Yang, Y. *et al*. Identification of metastasis and prognosis-associated genes for serous ovarian cancer. *Biosci. Rep.* **40**(6), 20194324 (2020).
43. Gomez-Roman, N., McGregor, F., Wheate, N. J. & Plumb, J. A. Cucurbit [7] uril encapsulated cisplatin overcomes resistance to cisplatin induced by Rab25 overexpression in an intraperitoneal ovarian cancer model. *J. Ovarian Res.* **8**, 62 (2015).
44. Huang, X. *et al*. Carrier-free multifunctional nanomedicine for intraperitoneal disseminated ovarian cancer therapy. *J. Nanobiotechnol.* **20**(1), 93 (2022).
45. Asare-Werehene, M. *et al*. Plasma gelsolin confers chemoresistance in ovarian cancer by resetting the relative abundance and function of macrophage subtypes. *Cancers (Basel).* **14**(4), 1039 (2022).
46. Dhuriya, Y. K. & Sharma, D. Necroptosis: A regulated inflammatory mode of cell death. *J. Neuroinflamm.* **15**(1), 199 (2018).
47. Vandenabeele, P., Galluzzi, L., Vanden Berghe, T. & Kroemer, G. Molecular mechanisms of necroptosis: An ordered cellular explosion. *Nat. Rev. Mol. Cell Biol.* **11**(10), 700–714 (2010).
48. Hong, X. *et al*. A novel prognostic model based on seven necroptosis-related miRNAs for predicting the overall survival of patients with lung adenocarcinoma. *Biomed. Res. Int.* **2022**, 3198590 (2022).
49. Negroni, A., Colantoni, E., Cucchiara, S. & Stronati, L. Necroptosis in intestinal inflammation and cancer: New concepts and therapeutic perspectives. *Biomolecules.* **10**(10), 1431 (2020).
50. Li, Y. *et al*. Identification of 5-(2,3-dihydro-1 H-indol-5-yl)-7 H-pyrrolo[2,3- d]pyrimidin-4-amine derivatives as a new class of receptor-interacting protein kinase 1 (RIPK1) inhibitors, which showed potent activity in a tumor metastasis model [published correction appears in J Med Chem. 2019 Mar 28;62(6):3169]. *J. Med. Chem.* **61**(24), 11398–11414 (2018).
51. Strilic, B. *et al*. Tumour-cell-induced endothelial cell necroptosis via death receptor 6 promotes metastasis. *Nature.* **536**(7615), 215–218 (2016).
52. Aaes, T. L. & Vandenabeele, P. The intrinsic immunogenic properties of cancer cell lines, immunogenic cell death, and how these influence host antitumor immune responses. *Cell Death Differ.* **28**(3), 843–860 (2021).

53. Jin, J., Li, Y., Muluh, T. A., Zhi, L. & Zhao, Q. Identification of CXCL10-relevant tumor microenvironment characterization and clinical outcome in ovarian cancer. *Front. Genet.* **12**, 678747 (2021).
54. Li, W., Ma, J. A., Sheng, X. & Xiao, C. Screening of CXC chemokines in the microenvironment of ovarian cancer and the biological function of CXCL10. *World J. Surg. Oncol.* **19**(1), 329 (2021).
55. Vilgelm, A. E. & Richmond, A. Chemokines modulate immune surveillance in tumorigenesis, metastasis, and response to immunotherapy. *Front. Immunol.* **10**, 333 (2019).
56. Dimitrakopoulos, F. D. *et al.* Expression of intracellular components of the NF-κB alternative pathway (NF-κB2, RelB, NIK and Bcl3) is associated with clinical outcome of NSCLC patients. *Sci. Rep.* **9**(1), 14299 (2019).
57. Shen, F. *et al.* RelB, a good prognosis predictor, links cell-cycle and migration to glioma tumorigenesis. *Oncol. Lett.* **15**(4), 4404–4410 (2018).
58. Zhang, Y. *et al.* HZ08 suppresses RelB-activated MnSOD expression and enhances radiosensitivity of prostate cancer cells. *J. Exp. Clin. Cancer Res.* **37**(1), 174 (2018).
59. Wang, Z. *et al.* Prognostic significance of mRNA expression of CASPs in gastric cancer. *Oncol. Lett.* **18**(5), 4535–4554 (2019).
60. Han, R., Yang, H., Lu, L. & Lin, L. Tiliroside as a CAXII inhibitor suppresses liver cancer development and modulates E2Fs/Caspase-3 axis. *Sci. Rep.* **11**(1), 8626 (2021).
61. Hong, W. *et al.* Immune-related lncRNA to construct novel signature and predict the immune landscape of human hepatocellular carcinoma. *Mol. Ther. Nucleic Acids.* **22**, 937–947 (2020).
62. Wang, T., Sun, J. & Zhao, Q. Investigating cardiotoxicity related with hERG channel blockers using molecular fingerprints and graph attention mechanism. *Comput. Biol. Med.* **153**, 106464 (2023).
63. Sun, F., Sun, J. & Zhao, Q. A deep learning method for predicting metabolite-disease associations via graph neural network. *Br. Bioinform.* **23**(4), bbac266 (2022).
64. Hu, H. *et al.* Modeling and analyzing single-cell multimodal data with deep parametric inference. *Br. Bioinform.* **24**(1), bbad005 (2023).
65. Zhang, L., Yang, P., Feng, H., Zhao, Q. & Liu, H. Using network distance analysis to predict lncRNA-miRNA interactions. *Interdiscip. Sci.* **13**(3), 535–545 (2021).
66. Chen, Z. *et al.* DCAMCP: A deep learning model based on capsule network and attention mechanism for molecular carcinogenicity prediction. *J. Cell. Mol. Med.* **27**(20), 3117–3126 (2023).
67. Meng, R., Yin, S., Sun, J., Hu, H. & Zhao, Q. scAAGA: Single cell data analysis framework using asymmetric autoencoder with gene attention. *Comput. Biol. Med.* **165**, 107414 (2023).
68. Zhao, J., Sun, J., Shuai, S. C., Zhao, Q. & Shuai, J. Predicting potential interactions between lncRNAs and proteins via combined graph auto-encoder methods. *Br. Bioinform.* **24**(1), bbac527 (2023).
69. Gao, H. *et al.* Predicting metabolite-disease associations based on auto-encoder and non-negative matrix factorization. *Br. Bioinform.* **24**(5), bbad259 (2023).
70. Li, X. *et al.* RIP1-dependent linear and nonlinear recruitments of caspase-8 and RIP3 respectively to necrosome specify distinct cell death outcomes. *Protein Cell.* **12**(11), 858–876 (2021).
71. Jin, J. *et al.* Quantifying the underlying landscape, entropy production and biological path of the cell fate decision between apoptosis and pyroptosis. *Chaos Solitons Fractals.* **178**, 114328 (2024).
72. Jin, J. *et al.* Biphasic amplitude oscillator characterized by distinct dynamics of trough and crest. *Phys. Rev. E.* **108**(6–1), 064412 (2023).

Acknowledgements

Author contributions

Y.L.Q. and Y.W.S. conceived and designed the study; Y.L.Q., Y.W.S. and M.X.R. searched the related articles; Y.L.Q., M.X.R., Z.T.H. and L.X. analyzed the data; Y.L.Q., M.X.R. and Z.T.H. wrote the manuscript. R.X.C. supervised the whole process. All authors read and approved the final manuscript.

Funding

Competing interests

The authors declare no competing interests.

Additional information

Supplementary Information The online version contains supplementary material available at https://doi.org/10.1038/s41598-024-61849-y.

Correspondence and requests for materials should be addressed to R.C.

Reprints and permissions information is available at www.nature.com/reprints.

Publisher's note Springer Nature remains neutral with regard to jurisdictional claims in published maps and institutional affiliations.